TELKOMNIKA Indonesian Journal of Electrical Engineering
Vol.12, No.6, June 2014, pp. 4427 ~ 4437
DOI: 10.11591/telkomnika.v12i6.5478

Motion Compensation Technique Based on Fractional Fourier Transform

Tan Gewei*, Pan Guangwu, Lin wei
School of information science and engineering, Huaqiao University, Xiamen, China
*Corresponding author, e-mail: tangewei70@163.com

Abstract

Fractional Fourier transform(FrFT) is a kind of generalized Fourier transform, which processes signals in the unified time-frequency domain and the linear frequency modulation signal can be well focused after FrFT. Motion error is an important factor affecting the SAR resolution, pointing to the problem that the effect of error elimination is not obvious in processing non-stationary motion error using the traditional FFT based motion compensation combined SAR imaging algorithm, FrFT based two-step motion compensation combined wavenumber domain algorithm and sub-aperture wide beam motion compensation algorithm are put forward in this paper, which are expected to eliminate the influence of motion error more effectively, so as to obtain high quality SAR images. The simulation results and the imaging results of real SAR data show that the proposed algorithms indeed eliminate the influence of motion error effectively. (The real SAR data provided by Institute of Electronics, Chinese Academy of Sciences).

Keywords: *fractional Fourier transform, motion error, two-step motion compensation, wide-beam motion compensation, high resolution*

1. Introduction

The system theory and related technology for SAR are established on keeping the flight path of radar platform in a straight line, but the atmospheric turbulence or other natural factors often make the aircraft deviated from the nominal track and generating motion error of antenna phase center, which will cause the amplitude modulation and phase modulation of radar echo signals, result in the image blurring and geometric distortions. In order to obtain high quality SAR images, the motion error must be compensated [1-3].

The earliest motion compensation scheme only considered space-invariant motion error [3], but with the require for high resolution, range-variant motion error must be considered, so two-step motion compensation techniques combined imaging algorithm is put forward to compensate such errors. With the development of low frequency radar, the effect of azimuth-variant motion error to the degeneration of SAR imaging quality is more and more significant [4], which presents a new problem for the motion compensation technique.

Fractional Fourier transform (FrFT) is proposed by V.Namias in 1980 [5], which is a new time-frequency analysis tool. Compared to the Fourier transform, FrFT has incomparable superiority in processing non-stationary signals and chirp signals. Chirp signal can be well focused after fractional Fourier transform with the specific rotation angle, which provides a possibility to achieve high resolution and high accuracy in SAR imaging. Especially when signal and interference source are coupled to each other, good separation effect in fractional domain can be obtained [6-8].

There has been literatures putting forward SAR imaging algorithm combining with FrFT. Literature [9] and [10] proposed an improving CS imaging algorithm based on FrFT. Literature [11] and [12] also proposed a combination of FrFT and RD imaging algorithm. These research results show that FrFT can contribute to the improvement of SAR resolution.

In order to eliminate the influence of motion error more effectively and improve the resolution, in the paper, FrFT is combined with the two-step motion compensation technology and SAR imaging algorithm, through utilizing the superiority of FrFT in processing chirp signal and non-stationary signal, so as to obtain high quality SAR images.

Received December 22, 2013; Revised February 15, 2014; Accepted February 27, 2014

2. Franctional Fourier Transform

The fractional Fourier transform and its inverse transform for signal $x(t)$ is defined as:

$$X_p(u) = F_p(x) = \int_{-\infty}^{\infty} x(t) K_p(t,u)\, dt \tag{1}$$

$$x(t) = F_{-p}(X) = \int_{-\infty}^{\infty} X_p(u) K_{-p}(t,u)\, du \tag{2}$$

Where,

$$K_p(t,u) = \begin{cases} \sqrt{\dfrac{1-j\cot\alpha}{2\pi}} \exp\left\{ j\pi\left((t^2+u^2)\cot\alpha - 2ut\csc\alpha \right) \right\} & \alpha \notin n\pi \\ \delta(t-u) & \alpha \in n\cdot 2\pi \\ \delta(t+u) & \alpha+\pi \in n\cdot 2\pi \end{cases} \tag{3}$$

And $p = \dfrac{2}{\pi}\alpha$, which is the order of FrFT. when $p=1$, FrFT is the Fourier transform.

The fractional Fourier transform for chirp signal is as follow:

$$X_p(u) = F_p(x) = \int_{-\infty}^{\infty} x(t) K_p(t,u)\, dt = A e^{j\pi u^2 \cot\alpha} \int_{-\infty}^{\infty} e^{j2\pi k t^2} e^{j\pi t^2 \cot\alpha - j2\pi ut\csc\alpha}\, dt \tag{4}$$

When,

$$\cot\alpha = -2k \ , \ F_{p_{opt}}\left[e^{j2\pi kt^2} \right] = k\delta(u) \tag{5}$$

$$p_{opt} = -\frac{2}{\pi} arc\cot(2k) \tag{6}$$

Where k is the coefficient of transform, p_{opt} is the optimal order of FrFT. Formula (5) shows, the optimal order FrFT for chirp signal is a impulse signal.

FrFT has the following time-shift and frequency-shift property,

$$F_p[s(t-\tau)](u) = \mathrm{e}^{j\pi\tau^2 \sin\alpha\cos\alpha - j2\pi u\tau\sin\alpha}\, F_p[s(t)](u-\tau\cos\alpha) \tag{7}$$

$$F_p[s(t)e^{j2\pi vt}](u) = \mathrm{e}^{-j\pi v^2 \sin\alpha\cos\alpha + j2\pi uv\cos\alpha}\, F_p[s(t)](u-v\sin\alpha) \tag{8}$$

According to the frequency-shift property, there is,

$$F_{p_{opt}}[\mathrm{e}^{j2\pi\left(kt^2+vt\right)}](u) = \delta(u - v\sin\alpha) \tag{9}$$

Where ignoring the coefficient, if the chirp signal is a discrete sequence, then the optimal order is:

$$p_{opt} = -\frac{2}{\pi} arc\cot\left(\frac{2k}{f_s^2 / N} \right) \tag{10}$$

In which, f_s as the sampling frequency, N as the sequence length.

Just using the optimal-order fractional Fourier transform, the chirp signal will be well focused, which no needs additional matching compression, thereby improving the processing efficiency.

3. Motion Error Mode and SAR Echo Signals with Motion Errors

The motion error refers to the difference of the distance from one target to real track and the distance from the target to the nominal track. By taking the target P in Figure 1, for example, the deviation from the nominal flight path is $(\Delta x(t), \Delta y(t), \Delta z(t))$, the real distance is $r(t)$ and the nominal distance is $R(t)$.

The slant range with motion error is,

$$r(t) = \sqrt{\left[\Delta x(t) + vt - x_0\right]^2 + \left[\Delta y(t) - y_0\right]^2 + \left[\Delta z(t) - z_0\right]^2} \tag{11}$$

Where $r_0 = \sqrt{y_0^2 + z_0^2}$, $y_0 = r_0 \sin\beta$, $z_0 = r_0 \cos\beta$, thus,

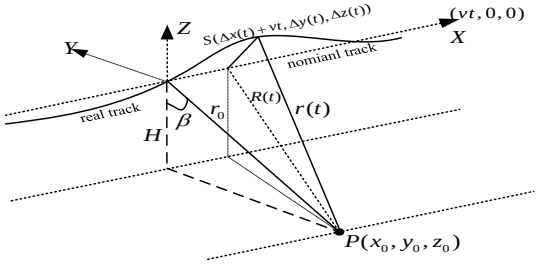

Figure 1. Geometry of SAR System under Side Mode

$$\begin{aligned} r(t) &= \sqrt{\left[\Delta x(t) + vt - x_0\right]^2 + \left[\Delta y(t) - r_0 \sin\beta\right]^2 + \left[\Delta z(t) - r_0 \cos\beta\right]^2} \\ &\approx r_0 + \frac{\left[\Delta x(t) + vt - x_0\right]^2}{2r_0} - \Delta y(t)\sin\beta - \Delta z(t)\cos\beta \\ &= R(t) + \Delta r_0(t) + \Delta r_{av}(t) \end{aligned} \tag{12}$$

Where $R(t) = \sqrt{r_0^2 + (vt - x_0)^2}$, which is the slant range without motion error.

$$\Delta r_0(t) = \Delta y(t)\sin\beta + \Delta z(t)\cos\beta = \Delta r_{ref}(t, r_{ref}) + \Delta r_{rv}(t, r_0) \tag{13}$$

Which is motion error in range direction and can be divided as range-invariant error Δr_{ref} and range-variant error Δr_{rv}. The azimuth error is:

$$\Delta r_{av}(t, x_0) = \frac{(vt - x_0)\Delta x(t)}{r_0} + \frac{\left[\Delta x(t)\right]^2}{2r_0} \tag{14}$$

The influence of motion error to different point target in azimuth direction as shown in Figure 2, when the azimuth error is Δx, the change of slant range is:

$$\Delta r_P = PS - PS_0 \approx \frac{(\Delta x)^2}{2r_0} \tag{15}$$

The range change of P_1 is:

$$\Delta r_{P_1} = P_1S - P_1S_0 = \sqrt{r_0^2 + (x_L - \Delta x)^2} - \sqrt{r_0^2 + x_L^2} \approx -\frac{(2x_L - \Delta x)\Delta x}{2r_0} \tag{16}$$

Where x_L is half of the synthetic aperture length, when azimuth beam is wide, the azimuth space-variant properties of motion error is obvious.

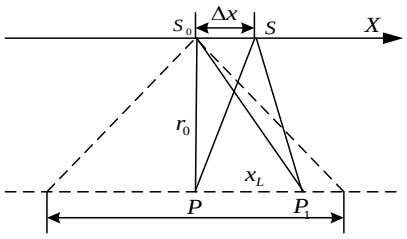

Figure 2. Motion Error for Different Point Target in Azimuth

Suppose that SAR transmit the chirps to an observed scene, their echoes after the demodulation are:

$$sd\left(t,\tau;r_0\right)=\sigma\left(x_0,r_0\right)\cdot rect\left(\frac{\tau-2r/c}{T_p}\right)\exp\left\{-j\pi k\left(\tau-\frac{2r}{c}\right)^2\right\}\cdot rect\left(\frac{t-t_0}{T_s}\right)\exp\left\{-j\frac{4\pi r}{\lambda}\right\} \quad (17)$$

Where τ is fast time in the slant range direction, t is slow time along the radar flight path, c and λ are the speed of light and the radar wavelength respectively, and k is the chirp rate. $rect()$ is the rectangle function, in which T_p and T_s are the pulse duration and synthetic aperture time. $r(t)$ is the instant range from the radar to a point target in the observed scene, which includes motion error.

$$r(t)=\sqrt{r_0^2+\left(vt-x_0\right)^2}+\Delta r_{ref}\left(t;r_{ref}\right)+\Delta r_{rv}\left(t,r_0\right)+\Delta r_{av}\left(t,x_0\right) \quad (18)$$

Ignore the azimuth motion error, the Fourier transform in the range direction first is performed by the stationary phase principle, the result is:

$$\begin{aligned}sD\left(t,f_r;r_0\right)=C_1\cdot\sigma\left(x_0,r_0\right)\cdot rect\left(\frac{f_r}{B_r}\right)\cdot rect\left(\frac{t-t_0}{T_s}\right)\cdot\exp\left\{j\pi\frac{f_r^2}{k}\right\}\cdot\exp\left\{-j\frac{4\pi r_0}{c}f_r\right\}\cdot\exp\left\{-j\frac{4\pi\Delta r_{ref}\left(t,r_{ref}\right)}{c}f_r\right\}\\ \cdot\exp\left\{-j\frac{4\pi r_0}{\lambda}\right\}\cdot\exp\left\{-j\frac{4\pi\Delta r_{ref}\left(t,r_{ref}\right)}{\lambda}\right\}\cdot\exp\left\{-j\varphi_{rv}\left(t;r_0\right)\right\}\end{aligned} \quad (19)$$

Range-invariant motion errors cause the echo envelope delay errors (third item) and azimuth phase errors (fifth item), which can be compensated along with range compress. Range-variant motion errors (sixth item) is related to slant range. In real SAR data, all point target are spread out in range direction and in azimuth direction, so compensation to such errors must be implemented after range compression and the range migration correction is completed.

4. Two-step Motion Compensation Combined Wavenumber Domain Algorithm Based on FrFT

Stolt interpolation is a key step in traditional two-step motion compensation combined wavenumber domain algorithm, which not only increases the amount of calculation, but also brings additional error. Fractional Fourier transform can replace the interpolation operation and can transform signal into range-Doppler domain at the same time, thus improving the calculation efficiency and imaging resolution.

Figure 3 is processing flow of the two-step motion compensation combined wavenumber domain algorithm based on FrFT.

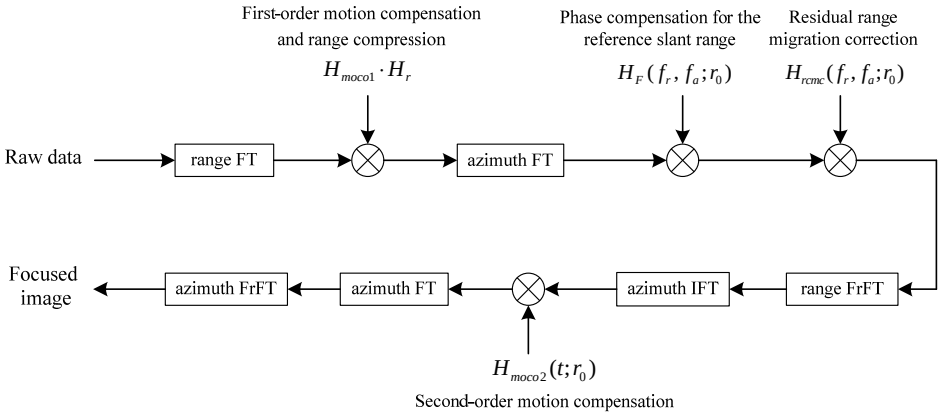

Figure 3. Processing Flow for the Two-step Motion Compensation Combined Wavenumber Domain Algorithm Based on FrFT

First the raw data is transformed into range frequency domain by Fourier transform in the range direction (range FT), then multiplying H_{moco1} and H_r to complete range focusing and first-order motion compensation.

$$H_{moco1} \cdot H_r = \exp\left\{ j \frac{4\pi \Delta r_{ref}\left(t, r_{ref}\right)}{c} \left(f_r + f_c \right) \right\} \exp\left\{ -\pi \frac{f_r^2}{K_r} \right\} \tag{20}$$

Next performing Fourier transform in the azimuth direction, signal is inverted into two-dimensional frequency domain, the result is:

$$SD(f_a, f_r; r_0) = C_2 \cdot \sigma \cdot rect\left[\frac{f_r}{B_r} \right] \cdot \exp\left\{ j\psi(f_a, f_r; r_0) \right\} \cdot rect\left[\frac{f_a}{B_d} \right] \cdot \exp\left\{ -j\varphi_{rv}\left(f_a; r_0 \right) \right\} \tag{21}$$

Where φ_{rv} is phase error caused by the range-variant motion error.

$$\psi(f_a, f_r; r_0) = -\frac{4\pi r_0}{\lambda} \sqrt{\left(1 + \frac{f_r}{f_c}\right)^2 - \left(\frac{\lambda f_a}{2v}\right)^2} \tag{22}$$

Which can be divided into two parts according the reference range,

$$\psi(f_a, f_r; r_0) = \psi_0(f_a, f_r; r_m) + \psi_1(f_a, f_r; r_0) \tag{23}$$

$$\psi_0(f_a, f_r; r_m) = -\frac{4\pi r_m}{\lambda} \sqrt{\left(1 + \frac{f_r}{f_c}\right)^2 - \left(\frac{\lambda f_a}{2v}\right)^2} \tag{24}$$

$$\psi_1(f_a, f_r; r_0) = -\frac{4\pi \delta r}{\lambda} \sqrt{\left(1 + \frac{f_r}{f_c}\right)^2 - \left(\frac{\lambda f_a}{2v}\right)^2} \tag{25}$$

Where $r_0 = r_m + \delta r,\ \delta r \in \left[-w_r / 2, w_r / 2\right],\ r_m$ is slant range of the swath middle, w_r is the swath wide.

$$\psi_0(f_a, f_r; r_m) = -\frac{4\pi r_m}{c}\left[f_c\gamma(f_a) + \frac{f_r}{\gamma(f_a)} - \frac{1-\gamma(f_a)^2}{2f_c\gamma(f_a)^3} f_r^2 + \frac{1-\gamma(f_a)^2}{2f_c^2\gamma(f_a)^5} f_r^3 + \cdots \right] \quad (26)$$

The first item corresponds to the azimuth compression, second to range cell migration, third to second range compression, the fourth is high-order coupling item of range and azimuth. So choosing the following compensation function,

$$H_F(f_a, f_r; r_m) = \exp\left\{ -j\psi_0(f_a, f_r; r_m) + \frac{4\pi r_m}{\lambda}\sqrt{1-\left(\frac{\lambda f_a}{2v}\right)^2} \right\} \quad (27)$$

Multiplying (21) with H_F can completing range cell migration correction, second range compression and phase compensation for high-order coupling item of range and azimuth for the reference range. The signal after this step is:

$$SD_{\delta r}(f_a, f_r; r_0) = C_2 \cdot \sigma \cdot rect\left[\frac{f_r}{B_r}\right] \cdot rect\left[\frac{f_a}{B_d}\right] \cdot \exp\{ j\psi_2(f_a, f_r; r_0)\} \cdot \exp\{-j\varphi_{rv}\} \quad (28)$$

$$\psi_2(f_a, f_r; r_0) = -\frac{4\pi r_0}{\lambda}\gamma(f_a) - \frac{4\pi\delta r}{c}\left[\frac{f_r}{\gamma(f_a)} - \frac{1-\gamma(f_a)^2}{2f_c\gamma(f_a)^3} f_r^2 + \frac{1-\gamma(f_a)^2}{2f_c^2\gamma(f_a)^5} f_r^3 + \cdots \right] \quad (29)$$

Then, multiplying H_{rcmc}, and performing fractional Fourier transform to invert signal into range-Doppler domain,

$$H_{rcmc}(f_r, f_a; r_0) = \exp\left\{ j\frac{4\pi\delta r}{c}\frac{f_r}{\gamma(f_a)} \right\} \quad (30)$$

$$Sd_1(f_a, \tau; r_0) = \int_{-\infty}^{+\infty} \left[SD_{\delta r}(f_a, f_r; r_0) \cdot H_{rcmc}(f_r, f_a; r_0) \right] K_p(f_r, \tau) df_r$$

$$= C_3 \cdot rect\left[\frac{f_a}{B_d}\right] \int_{-\infty}^{+\infty} rect\left[\frac{f_r}{B_r}\right] \exp\{ j\psi_2(f_a, f_r; r_0)\} \cdot \exp\left\{ j\pi\left((f_r^2 + \tau^2)\cot\alpha - 2f_r\tau\csc\alpha \right) \right\} df_r$$

$$= C_4 \cdot \sigma \cdot rect\left[\frac{f_a}{B_d}\right] \cdot \exp\left\{ -j\frac{4\pi r_0}{\lambda}\gamma(f_a) \right\} \cdot \exp\{-j\varphi_{rv}\} \cdot \sin c\left(\tau - \frac{2r_0}{c} \right) \quad (31)$$

Where $\alpha = -arc\cot\left(\frac{2\delta r}{c} \cdot \frac{1-\gamma(f_a)^2}{f_c\gamma(f_a)^3} \right)$, the optimal order of FrFT is $p_{opt} = \frac{2}{\pi}\alpha$.

Next, performing azimuth Fourier transform into two-dimensional time-domain, implementing second-order motion compensation, the corresponding phase compensation function is:

$$H_{moco2}(t, r_0) = \exp\left\{ j\left(\varphi_{mo}(t, r_0) - \frac{4\pi}{\lambda}\Delta r_{ref}(t, r_{ref}) \right) \right\} \quad (32)$$

Where φ_{mo} is phase error generated by motion error of different range.

Finally, in range-Doppler domain, completing azimuth compression by using FrFT and get focused image. The result is:

$$sd(t, \tau; r_0) = \int_{-\infty}^{+\infty} Sd_2(f_a, \tau; r_0) \cdot K_p(f_a, t) df_a$$

$$= C_5 \cdot \sigma \cdot \sin c(\tau - \frac{2r_0}{c}) \int_{-\infty}^{+\infty} rect\left[\frac{f_a}{B_d}\right] \cdot \exp\left\{-j\frac{4\pi r_0}{\lambda}\gamma(f_a)\right\} \cdot \exp\left\{j\pi\left((f_a^2 + t^2)\cot\beta - 2f_a t \csc\beta\right)\right\} df_a$$

$$= C_6 \cdot \sigma \cdot \sin c(\frac{t}{\sin\beta}) \cdot \sin c(\tau - \frac{2r_0}{c}) \quad (33)$$

Where, $\gamma(f_a) = \sqrt{1 - \left(\frac{\lambda f_a}{2v}\right)^2} \approx 1 - \frac{1}{2}\left(\frac{\lambda f_a}{2v}\right)^2$ and $\beta = \cot^{-1}\left(\frac{\lambda r_0}{2v^2}\right)$, the optimal order of FrFT is $p_{opt} = \frac{2}{\pi}\beta$.

5. Compensation to the Residual Motion Error in the Azimuth Direction

For low frequency radar, the space-variant property of motion error in the azimuth direction cannot ignore, how to eliminate the residual azimuth motion error is crucial to realize high resolution. The sub-aperture motion compensation algorithm for wide-beam SAR provides a way to resolve such problem.

When azimuth beam is wide, it is natural to divide the aperture into several so that the motion errors in the same sub-aperture are considered equal. Figure 4 shows the relation of azimuth position and azimuth motion error, L_s is the synthetic aperture, ΔL_i is sub-aperture, θ_i is squint angle which is one by one corresponding to azimuth position, so the motion error of every sub-aperture is also one by one corresponding to the squint angle.

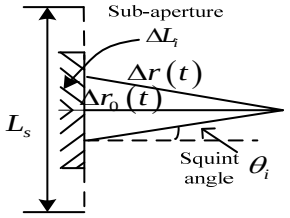

Figure 4. Relation of Azimuth Motion Error and Squint Angle

The azimuth residual motion error is:

$$\Delta r_{av} = \Delta r(t) - \Delta r_0(t) = \frac{\Delta r_0(t)}{\cos(\theta_i)} - \Delta r_0(t) \quad (34)$$

And the corresponding phase compensation function is:

$$H_{avmoco} = \exp\left\{j\frac{4\pi\Delta r_{av}}{\lambda}\right\} = \exp\left\{j\frac{4\pi\Delta r_0}{\lambda}\frac{(1-\cos\theta_i)}{\cos\theta_i}\right\}$$

$$= \exp\left\{j\frac{4\pi\Delta r_{ref}}{\lambda}\frac{(1-\cos\theta_i)}{\cos\theta_i}\right\} \cdot \exp\left\{j\frac{4\pi\Delta r_{rv}}{\lambda}\frac{(1-\cos\theta_i)}{\cos\theta_i}\right\} \quad (35)$$

The processing for the sub-aperture wide-beam motion compensation algorithm combining with two-step motion compensation is shown as Figure 5, after the second-order motion compensation, in range-Doppler domain, dividing the data into suitable size blocks, then performing motion compensation for each block data with 35 [13].

When $\frac{4\pi}{\lambda} \cdot |\Delta r_{rv}| << 1$, the range-variant motion error can be ignored, the processing for the sub-aperture wide beam motion compensation algorithm is shown as Figure 6.

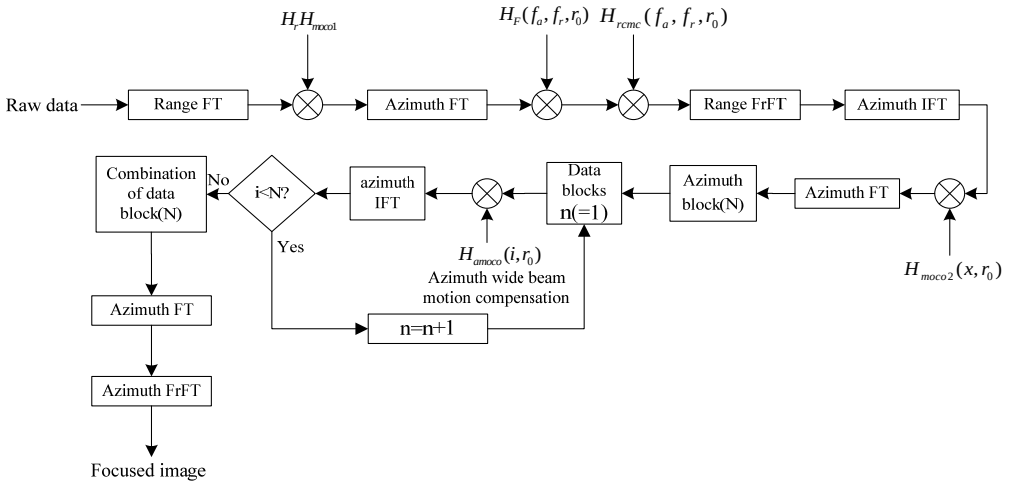

Figure 5. Processing of Sub-aperture Wide Beam Motion Compensation Algorithm Combining with Two-step Motion Compensation

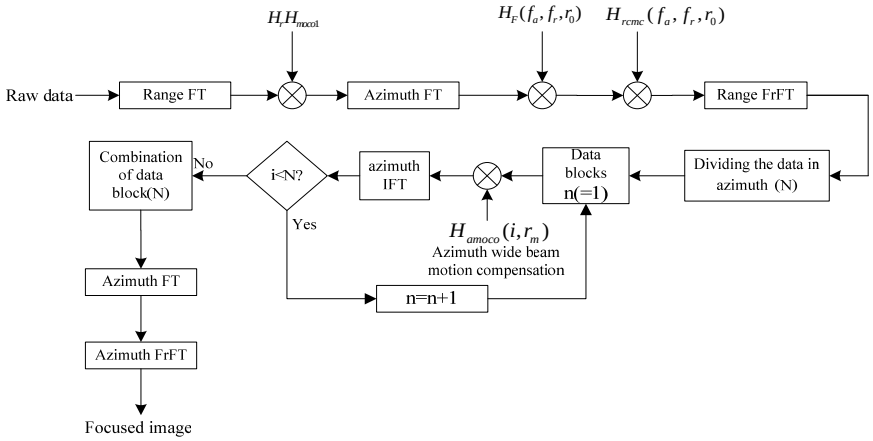

Figure 6. Processing for Sub-aperture Wide Beam Motion Compensation Algorithm Combinig with Two-step Motion Compensation while the Range-variant Motion Error is Ignored

6. Simulations and SAR Imaging Results Based on Real Data for the Proposed Algorithm

6.1. Simulation Results to Point Target with Motion Error in the Range Direction for the Algorithm

Simulation results for the proposed algorithm are as follow, the simulation parameters as shown in Table 1.

Table 1. Simulations Parameters

Parameter	value
Carrier frequency	1.5GHz
Bandwidth for transmit signal	150MHz
Pulse duration of transmit signal	1.5μs
The number of range sampling points	1024
Forward velocity	180m/s
Length of synthetic aperture	320m
The number of azimuth sampling points	512
Range-invariant motion error	t^2

The range error is non-stationary random motion error whose mean value is exponential function, so range-variant motion error is:

$$\Delta r_{rv}\left(t, r_0\right) = \Delta r_0\left(t, r_0\right) - \Delta r_{ref}\left(t, r_{ref}\right)$$

Simulations to point target with motion error using FFT based the two-step motion compensation combined wavenumber domain algorithm and FrFT based the two-step motion compensation combined wavenumber domain algorithm are shown in Figure 7, (a) is comparison of azimuth impulse response with no error and after motion compensation using traditional algorithm; (b) is comparison of azimuth impulse response with no error and after motion compensation using the proposed algorithm; (c) is comparison of range impulse response after motion compensation by the two algorithm; (d) is comparison of azimuth impulse response after motion compensation by the two algorithm.

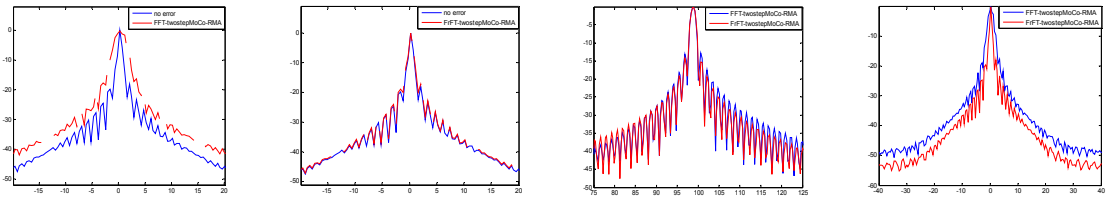

(a) (b) (c) (d)

Figure 7. Comparing of Impulse Response between No Error and with Error after Compensation

Figure 7(b) shows that the main lobe of impulse response in azimuth direction is narrower and the influence of quadratic phase error is eliminated virtually. The wider mainlobe of Figure 7(a) indicates the influence of quadratic phase error still exists, which proves the processing effect of non-stationary motion error using FrFT is obvious than FFT, at the same time proves that the focusing effect of chirp signal using FrFT is better than FFT. The performance comparison of their impulse response in the azimuth is shown in Table 2.

Table 2. Performance Comparison of Impulse Response in Azimuth Direction

Motion compensation algorithm	The wide of main lobe	Integrated side lobe ratio	Peak to side lobe ratio
No motion compensation when no error	1.10m	-26.012 dB	-31.432dB
FFT-twostep motion compensation RMA	4.864m	-24.681dB	-24.218dB
FrFT-twostep motion compensation RMA	1.125m	-25.589dB	-30.353dB

6.2. Imaging Results Comparison for the Proposed Algorithm and the Traditional Algorithm

Figure 8(a) is the imaging result of the real SAR data with motion errors, the blurring image shows there are obvious quadratic phase errors. Processing result for such SAR data using the traditional FFT based two step motion compensation wavenumber domain algorithm is shown in Figure 8(b), due to the elimination of most motion error, image resolution is improving significantly, but in some places with more details (such as part of the circle line), the image is not clear and image resolution deteriorates because of the residual phase error. The processing result with the proposed FrFT based two step motion compensation wavenumber domain algorithm is shown in Figure 8(c), details information increases, the image resolution is further improving.

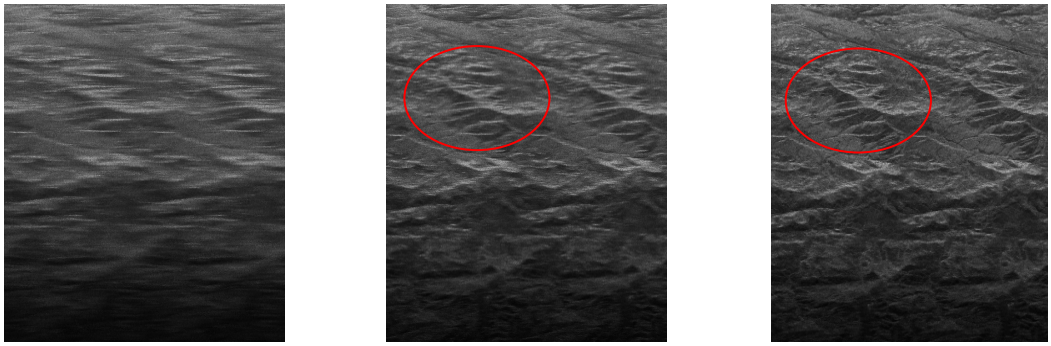

(a) (b) (c)

Figure 8. Comparison of Imaging Results before and after Motion Compensation

6.3. Simulations for the Sub-aperture Wide Beam Motion Compensation Algorithm

Figure 9(a) is the imaging results for L-SAR data with motion error, the fuzzed image shows there are complex motion error in the data; Figure 9(b) is the processing results by the two-step motion compensation combined wavenumber domain algorithm, due to the elimination of the motion error in the range direction, the focusing performance of the image is remarkably improved; Figure 9(c) is processing results by the sub-aperture wide beam motion compensation algorithm, the residual motion errors in azimuth direction are further eliminated, so the image is more clear. the image size is: 2048×4096 , resolution is: $2.4m \times 2.4m$.

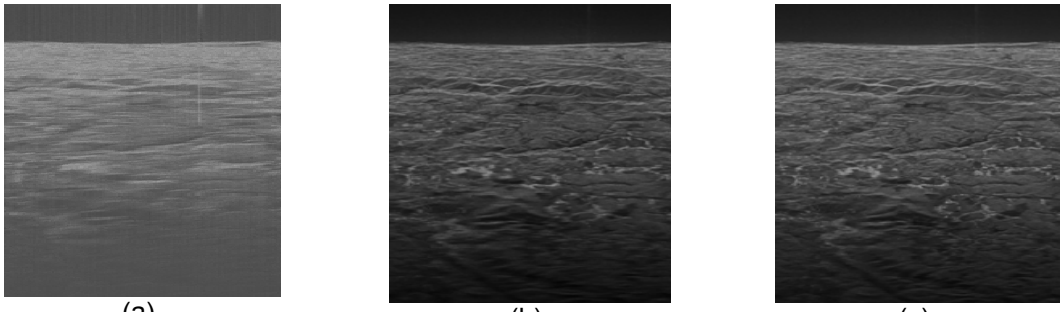

(a) (b) (c)

Figure 9. Identification of Flux Sector and Determination of the Appropriate Flux Error Status in the Block of Modification of Flux Error Status

7. Conclusion

Motion error is a crucial factor to limit airborne SAR resolution improving [14, 15]. As modern SAR systems are continuously developing into the direction of higher spatial resolution, how to overcome the motion error caused by air turbulence is an urgent problem to radar workers. The two-step motion compensation combined wavenumber domain algorithm based on fractional Fourier transform and the sub-aperture wide beam motion compensation algorithm based on FrFT proposed in this paper can solve various motion errors effectively, especially can eliminate the image blurring caused by non-stationary motion errors, the research provides an effective solution scheme for motion error.

Acknowledgements

This project is supported by the natural science foundation of Fujian province of 2013 project (2013J01242).

References

[1] Yan-lei Li, Xing-dong Liang, et al. A Motion Compensation Approach Integrated in the Omega-K Algorithm for Airborne SAR. *IEEE International Conference on Imaging Systems and Techniques*. 2012; 1: 245-248.

[2] Yongfei Mao, Maosheng Xiang, et al. *Error Analysis of SAR Motion Compensation*. IEEE International Conference on Imaging Systems and Techniques. 2012; 1: 377-380.

[3] Hao Guo, Yang Li. *Studying Atmospheric Turbulence Effects on Aircraft Motion for Airborne SAR Motion Compensation Requirements*. IEEE International Conference on Imaging Systems and Techniques. 2012; 1: 152-157.

[4] Yan-lei Li, Xing-dong Liang, et al. Improvements to the Frequency Division-Based Sub-aperture Algorithm for Motion Compensation in Wide-Beam SAR. *IEEE Geoscience and remote sensing letters.* 2013; 10(5): 1219-1223.

[5] V. Namias. The Fractional Fourier Transform and Its Application in Quantum Mechanics. *Journal of Inst. Math.* 1980; 25: 241-265

[6] Qi lin, Tao Ran, et al. *Adaptive Time-Varying Filter for Linear FM Signal in Fractional Fourier Domain.* 6th IEEE International Conference on Signal Processing. 2002; 2: 1425-1428.

[7] Durak L, Aldirmaz S. Adaptive Fractional Fourier Domain Filtering. *Signal Processing*. 2010; 90(4): 1188-1196.

[8] Ervin S, Igor D, LJubia S. Fractional Fourier Transform as a Signal Processing Tool: An Overview of Recent Developments. *Signal Processing*. 2011; 91(6): 1351-1369.

[9] Amein AS. A New Chirp Scaling Algorithm Based on the Fractional Fourier Transform. *IEEE Signal Processing Letters*. 2005; 12(10): 705-708.

[10] Ahmed S Amein, John J Soraghan. Azimuth Fractional Transformation of the Fractional Chirp Scaling Algorithm. *IEEE Trans. on Geosciences and Remote Sensing.* 44(10): 2871-2879.

[11] Carmine Clemente, John J Soraghan. Range Doppler and chirp scaling processing of synthetic aperture radar data using the fractional Fourier transform. *IET Signal Processing*. 2012; 6(5): 503-510.

[12] MG El-Mashed, MI Dessouky. Target Image Enhancement in Radar Imaging Using Fractional Fourier Transform. *Sens Imaging.* 2012; 13: 37-53.

[13] Tan Gewei, Deng yunkai. The two-dimensional spatial-variant properties of airborne SAR motion error and its compensation. *Journal of electronics and information technology*. 2009; 31(2): 366-369.

[14] R Lanari, G Fornaro. A short discussion on the exact compensation of the SAR range-dependent range cell migration effect. *IEEE Transactions on Geoscience and Remote Sensing*. 1997; 35: 1446-1452.

[15] Jianzhao Huang, Jian Xie, Hongcai Li, Gui Tian, Xiaobo Chen. Self-adaptive Decomposition Level De-noising Method Based on Wavelet Transform. *TELKOMNIKA Indonesian Journal of Electrical Engineering*. 2012; 10(5): 1015-1020.